RSC Advances

ROYAL SOCIETY OF CHEMISTRY

www.rsc.org/advances

Cite this: DOI: 10.1039/c0xx00000x

www.rsc.org/xxxxxx

ARTICLE TYPE

Tailoring optical, magnetic and electric behavior of lanthanum strontium manganite $La_{1-x}Sr_xMnO_3$ (LSM) nanopowders prepared via co-precipitation method with different Sr^{2+} ion contents

Ali Omar Turky[*a,c], Mohamed Mohamed Rashad[a], Ali Mostafa Hassan[b], Elsayed M. Elnaggar[b], Mikhael Bechelany[c]

Received (in XXX, XXX) XthXXXXXXXXX 20XX, Accepted Xth XXXXXXXXX 20XX
DOI: 10.1039/b000000x

Lanthanum strontium manganite (LSM) nanopowders $La_{1-x}Sr_xMnO_3$ (x = 0.2, 0.5, 0.8) have been synthesized using the co-precipitation method based on methyl amine as a base at pH value 12. The effect of Sr^{2+} ion concentration on the crystal structure, microstructure, optical, magnetic and the electrical properties was investigated. Typically, in all of the formed LSM powders, XRD revealed that a pure single perovskite LSM phase was obtained after annealing at 1000°C for 2 h. This temperature was relatively low compared to what has been reported elsewhere. The microstructure of the produced LSM nanopowders depends from the Sr^{2+} concentrations. The observations of these powders confirmed their rough surface. Meanwhile, the transmittance of the sample was around 40 % for LSM with Sr^{2+} ratio of 0.8. Furthermore, the band gap energy of this powder was 2.6 eV. The refractive index was decreased with enhanced the Sr^{2+} ion content. Indeed, the saturation magnetization of the LSM powders was increased with increasing the Sr^{2+} ion concentration. Electrochemical impedance spectroscopy (EIS) evinced that the electrode specific polarization resistance of LSM samples was increased by increasing Sr^{2+} ion concentrations from 3.10 to 8.56 Ω cm^2.

A. Introduction

Strontium doped lanthanum manganite $La_{1-x}Sr_xMnO_3$ (LSM) perovskites are the principal component of the neoteric materials for the Solid oxide fuel cell (SOFC) cathodes. LSM-based compositions are showed interesting electrochemical properties for oxygen activation at high temperatures while they are thermo-chemically compatible with the widely used YSZ electrolyte material.[1] The $La_{0.8}Sr_{0.2}Mn0_3$ gives a good combination of electronic conductivity and expansion coefficient matching, and it is now available commercially for SOFC applications. Higher conductivity can be obtained at higher dopant levels, but the expansion coefficient then becomes overly high.[2-7] However, the polarization resistance of LSM dramatically increases with the decreasing operation temperature (1Ω cm^2 at 1000°C to 2000 Ω cm^2 at 500°C), which seriously limits the overall cathode performance at the intermediate temperature.[8] Besides, it has also reported that the electrochemical reactions of cathode materials, such as the LSM have proved to be very poor oxide ion conductors, but their electronic conductivity is high enough to make them attractive SOFC cathode material, which is particularly interesting when the strontium content is in the range of 0.1 to 0.3.

Otherwise, strontium doped lanthanum manganite $La_{1-x}Sr_xMnO_3$ has been widely used as magnetic sensors, read heads, information storage and actuations, automotive exhaust control, elimination of CO pollutant and as cathodes in solid oxide fuel cells (SOFC).[9, 10] Such extensive applications are attributed to their fascinating magneto-transport properties like colossal magneto resistance (CMR) coupled with excellent electrical, thermal, chemical and mechanical characteristics.[11] The microstructure and the homogeneity characteristics of LSM depend to a large extent on the processing conditions and are hard to control in the conventional ceramic synthesis process, which is based on the diffusion of the components in the solid state at high temperatures. For this reason alternative preparation routes for LSM synthesis based on wet chemical methods have been proposed.

A characterization of perovskite powders for the cathode and oxygen membranes prepared by different chemical routes was made by Sefir *et al.*[12] Indeed, there are several routes to synthesize perovskite structured materials. These routes include solid-state reaction,[13] co-precipitation,[14] sol-gel,[15] pyrolysis,[16] combustion and Pechini method.[17-19] In this context, conventional solid-state reaction route requires high calcination temperatures and long annealing times which often results in agglomerated coarse particles and subsequently problems for achieving uniform distribution of particles for particular applications such as SOFCs cathodes.[15] In comparison, wet chemical routes often results in almost pure phase with uniform distribution as well as high surface area without any consequently grinding as observed in solid state reaction strategy. Among the chemical routes, the

chemical co-precipitation method ensures proper distribution of the various metals ions resulting to stoichiometric and smaller particles size product, compared to some of the other procedures. Moreover, the chemical co-precipitation method is a low-cost technique suitable for mass production. Besides, it is even found that the rate of addition of precipitating agent could have a significant effect on the shape and size of the final powders.[20, 21] Herein, the aim of this article is to describe a versatile and cheap co-precipitation strategy to obtain $La_{1-x}Sr_xMnO_3$ nanoparticles at different Sr^{2+} ion contents using methyl amine as a base for the first time. The impact of Sr^{2+} ion molar ratio on the structural, microstructure as well as optical, magnetic, and electrical properties, of the newly synthesized system was further investigated in details using different physical approaches.

B Materials and Methods

1. Materials

All the chemicals used in this study such as lanthanum nitrate hexahydrate $La(NO_3)_3.6H_2O$ (Fluka) Analytical, anhydrous strontium nitrate $Sr(NO_3)_2$ (Sigma-Aldrich), manganese acetate tetrahydrate $C_4H_6MnO_4$ (AppliChem), and methylamine as a base were used as received. Moreover, deionized water was used in the whole work.

2. Procedure

Lanthanum strontium manganite (LSM) nanopowders were synthesized through co-precipitation strategy by mixing aqueous solutions of lanthanum nitrate hexahydrate $La(NO_3)_3.6H_2O$, anhydrous strontium nitrate $Sr(NO_3)_2$ and manganese acetate tetrahydrate $C_4H_6MnO_4$. Then, methyl amine solution as a base was gradually added to the mixture. Dark brown precipitate was formed. The formed precipitated precursors were filtered, washed with deionized water and ethanol. Thereafter, it was dried at 60 °C temperature for 24 h to form the hydroxide precursors. Finally, the powder samples were annealed at 1000°C at rate of 10 °C/min in static air atmosphere and maintained at the temperature for annealed time of 2 h.

3. Physical Characterization

X-ray powder diffraction (XRD) was carried out on a model Bruker AXS diffractometer (D8-ADVANCE Germany) with Cu Kα (λ = 1.54056 Å) radiation, operating at 40 kV and 40 mA. The diffraction data were recorded for 2θ values between 10 and 80°. Field emission scanning electron microscopy was performed by a FE-SEM (JEOL-JSM-5410 Japan). The UV-Vis absorption spectra were measured by UV-Vis-NIR-scanning spectrophotometer (JASCO V-570 spectrophotometer, Japan; Figure S1). The Dynamic Light Scattering (DLS) was measured using HORIBA LB-500 Particle Size Distribution Analyzer in the range from 3 to 6000 nm in a fixed angle 90° quartz cells. The magnetic properties of the prepared cobalt ferrite were measured at room temperature using vibrating sample magnetometer (7400-1 VSM, Lake Shore Co., Ltd., USA) with Integrated IDEAS VSM software at room temperature in a maximum applied field of 20 KOe. From the obtained hysteresis loops, the saturation magnetization (*Ms*), remanence magnetization (*Mr*) and coercivity (*Hc*) were determined. Electrochemical impedance spectrums (EIS) were recorded as a function of frequency with 6 points with an AC perturbation signal of 50 mA using a PARSTAT 4000 Potentiostat/Galvanostat/EIS Analyzer.

C. Results and Discussion

1. Crystal structure

The XRD after thermal treatments at 1000ºC for LSM with different Sr^{2+} ion contents are depicted in Figure 1. A low crystallized size powder was obtained at low strontium ion molar ratio. The crystallinity of the LSM samples was improved as the Sr^{2+} ion content was increased. Distinctly, all the XRD patterns showed that no excess impurity phases of La_2O_3 or $La(OH)_3$ was detected. Evidently, the nanoparticles were indexed as a single-phase perovskite LSM structure at different Sr^{2+} ion concentrations. Obviously, the data are in agreement with the Joint Committee on Powder Diffraction Standards card for LSM (JCPDS # 49-0595). There is no difference in the XRD patterns for the fifferent LSM powders. The crystallite size of the formed powders was estimated from the most intense peak (024) plane of XRD patterns based on Scherrer formula. Apparently, the crystallite size was Sr^{2+} ion dependent. It was increased with further increasing of Sr^{2+} ion content. The substitution of La^{3+} cation (1.36 Å) by a larger one Sr^{2+} (1.44 Å) led to the progressive increase in the number of holes from Mn^{3+} to Mn^{4+}. Subsequently, the substitution of La 3p by Sr 2p increases the content of Mn^{4+} ions to keep the charge neutrality[17, 18, 22].

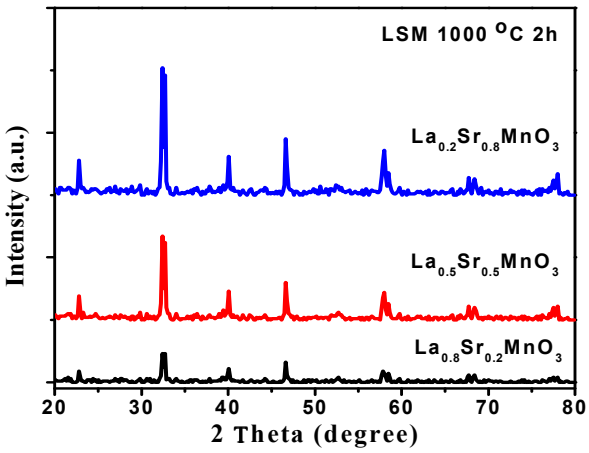

Fig. 1 XRD patterns of the LSM powder synthesized using co-precipitation method using methyl amine as a base at pH 2 then annealed at 1000 °C for 2 h with different Sr^{2+} ion concentrations

2. Microstructure

Figure 2 shows the morphologies of LSM samples prepared via co-precipitation method annealed at 1000°C for 2 h with different Sr^{2+} ion contents. At low Sr^{2+} content (Figure 2a), it can be seen that the particles were exhibited as tablet like structure with homogeneous small size and hard agglomerated. However, non-spherical faceted powders were displayed with Sr^{2+} ion molar

ratio of 0.5 as depicted in Figure 2b. Further increasing the Sr^{2+} ion ratio to 0.8 was found to form agglomerated faceted powders. Meanwhile, the microstructure observation performed for the samples indicated that the grain size was increased with increasing the Sr^{2+} ion concentrations. The grain size was increased from 45 nm at Sr^{2+} molar ratio of 0.2 to 113 nm at Sr^{2+} content 0.8. These results have been confirmed by DLS measurement (Figure SI2).

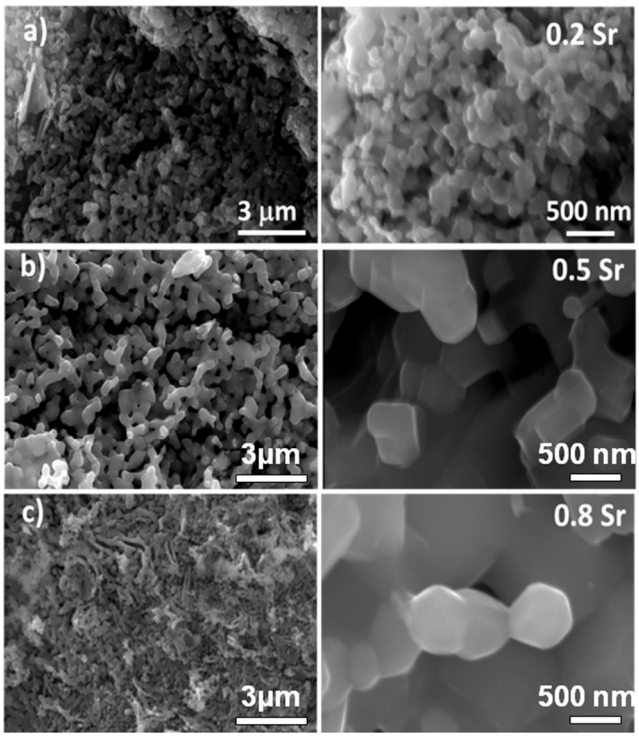

Fig. 2: Different magnifications of SEM images for lanthanum strontium manganite synthesized using co-precipitation method with different Sr^{2+}ion molar ratios and annealed at 1000° C for 2 h

3. Optical properties

Transmittance and absorbance spectra of the synthesized lanthanum strontium manganite nanopowders are shown in Figures 3 and 4. The transmittance curves exhibited typical induced interference fringes, a quite rapid fall-off at the lower wavelengths and good transparency response through the examined spectral range. The highest average transparency was associated to high Sr^{2+} ion concentration. A blue-shift of the transmittance-curve edge can be observed as Sr^{2+} ion content increases from 0.2 to 0.8. This explanation could be misleading due to spectra overlapping around the transmittance edge (below 400 nm) and occurrence of a knee-feature (at 200-300 nm).[23,24] The transmittance percentage is halved (nearly 40 %) by increasing the Sr^{2+} ion molar ratios. However, it is still good in the visible range and consistent with other reports available in literature. [24-26] This transmittance was found to be very appropriate for OLED applications.

The steep shape of the optical absorption spectra indicates that the visible light adsorption could be not caused by a transition from the impurity levels but was caused by the band-gap transition. The absorption band contains a tail extending rightwards until about 700 nm. This may result from the crystal defects formed during the growth of the LSM nanopowders. It is flat in the 400–800 nm range. It is noted that the lower UV cutoff of all samples appears at 300 nm and there is no remarkable absorption in the entire region of the spectrum. The spectrum clearly shows that the powders possess good optical absorbance 0.8 from 200 to 300 nm which is useful for second harmonic generation. By increasing the wavelength region to 400 nm, the absorbance was increased to 1.0 for all the prepared samples.[27]

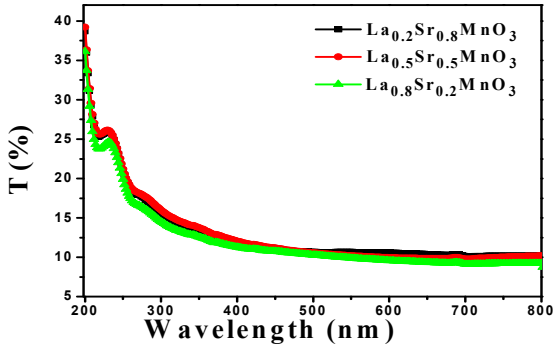

Fig. 3: Transmittance spectrum of LSM nanopowders synthesized using co-precipitation method using methyl amine as a base at pH 12 with varied the Sr^{2+} ion ratios (x=0.2, 0.5 and 0.8) annealed at 1000°C for 2 h

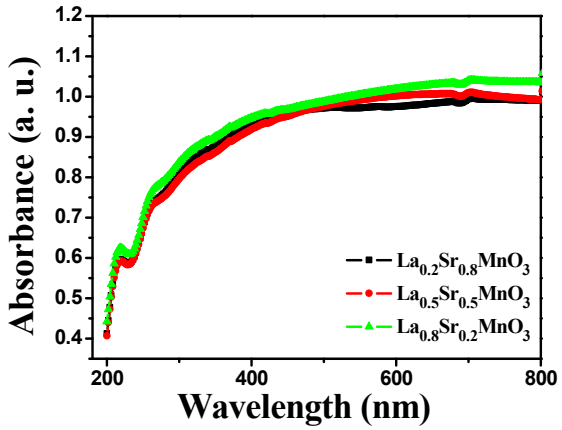

Fig. 4: Absorbance spectrum of LSM nanopowders synthesized using co-precipitation method using methyl amine as a base at pH 12 with varied the Sr^{2+} ion ratios (x=0.2, 0.5 and 0.8) annealed at 1000°C for 2 h

4. Band gap energy measurement

Here, the influence of the Sr^{2+} ion molar ratios on the band-gap energy of lanthanum strontium manganite has been investigated. hυ is the photon energy and Eg is the energy of the optical transition corresponding to the optical band gap. Value of the exponent n depends on the nature of the optical transition and takes the value of 1/2, 2, 3/2, or 3 for the direct-allowed, indirect-allowed, direct-forbidden or indirect forbidden transitions, respectively. The $[F(R\infty)h\upsilon]^{1/n}$ vs $h\upsilon$ plot shows the linear nature near the absorption edge for n =2 as shown in Figure 5. The

band-gap energy (*Eg*) was evaluated by Wood–Tauc theory[28,29] as plotted in Figure 5. The best linear relation of $\alpha h\upsilon \propto (h\upsilon\text{-}Eg)^n$ was determined as for *n* value of 2, indicating that this is an indirect allowed electronic transition. The band gap of the LSM nanopowders is calculated to be about 2.2 eV for $La_{0.8}Sr_{0.2}MnO_3$, 2.4 eV for $La_{0.5}Sr_{0.5}MnO_3$ and 2.6 eV for $La_{0.2}Sr_{0.8}MnO_3$ as shown in Figure 5. Such a value of the band gap energy suggests that these compounds may be a potential candidate for new high frequency optoelectronic devices, since the materials having the band gap energy greater than 2 eV is of particular interest in the UV region of the spectrum.[30, 31]. These values were nearly similar to the previous published by Tanguturi *et al.*[32] for $Nd_{0.7}Sr_{0.3}MnO_3$ thin film in which they were found to be 2.64 and 2.98 eV for deposited and annealed film. Cesaria *et al.*[27] have reported that the direct band gap energy of $La_{0.7}Sr_{0.3}MnO_3$ thin film deposited by pulsed laser deposition under different oxygen pressures was in the range between 2.44 to 3.5 eV. The change in band gap energy has been attributed to the change of Mn^{4+}/Mn^{3+} ratio as the function of La/Sr ratio according to the chemical formula $La^{3+}_{(1-x)}Sr^{2+}_{x}Mn^{3+}_{(1-x)}Mn^{4+}_{x}O_3$. Moreover, the Mn valence also depend on the oxygen concentration, based on the requirement of charge neutrality within the LSMO unit cell $La^{3+}_{(1-x)}Sr^{2+}_{x}Mn^{3+}_{(1-x+2\delta)}Mn^{4+}_{(x-2\delta)}O^{2-}_{(3-\delta)}$).

The results can be expressed on the basis of the band-structure states involved in LSMO optical response are the spin-unpolarized O2p-states and the Mn d-like states which split into low-lying narrower t_{2g} and high-lying broader e_g sub bands. Each of these sub bands further split into up- and down-spin bands due to the exchange-interaction. The Mn e_g bands (*i.e.* the doublet e^1_g and e^2_g) and the O2p levels are involved in the so-called charge transfer transitions: the dipole allowed d–d transitions between different Mn sites (the inter-atomic charge transfer transitions $Mn^{3+}(e^1_g) \rightarrow Mn^{3+}(e^2_g)$ and $Mn^{3+}(e^1_g) \rightarrow Mn^{4+}(e_g)$) and the dipole allowed transition between an O 2p-like state and a Mn d-like (O 2p $\rightarrow Mn^{3+}(e^2_g)$ and O 2p $\rightarrow Mn^{4+}(e_g)$ [27].

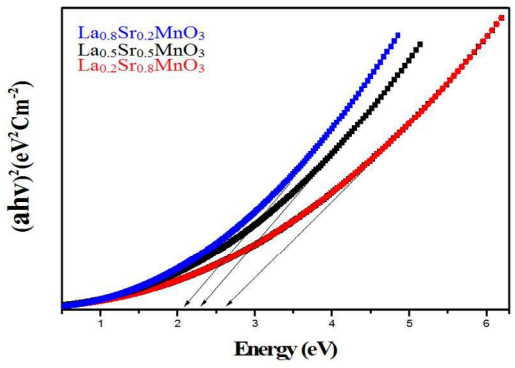

Fig. 5 The optical band gap energy value of the LSM nanopowders synthesized using co-precipitation method with different Sr^{2+}ion molar ratios and annealed at 1000°C for 2 h.

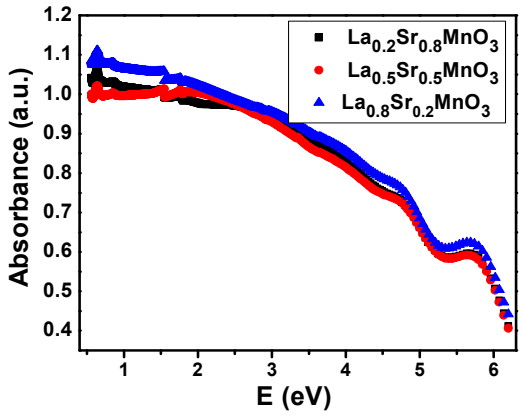

Fig. 6 Absorption spectra as a function of photon energy for LSM nanopowders prepared via co-precipitation method at calcinations temperature of 1000°C with different Sr^{2+} ion molar ratios (0.2, 0.5, and 0.8).

5. The refractive index

The refractive index of the samples is calculated using Moss relation[33]

$$\mathbf{E_g\, n^4 = 95\ eV} \qquad \textit{(Equation 1)}$$

Where Eg is the energy band gap. The refractive index of the samples is also calculated using a different relation presented by Herve and vandamme as: [34]

$$\mathbf{n} = \sqrt{1 + \left(\frac{A}{E_g + B}\right)^2} \qquad \textit{(Equation 2)}$$

Where A and B are the numerical constants with values of 13.6 eV and 3.4 eV respectively. The refractive index was slightly decreased with increasing the Sr^{2+} ion content. The results can be discussed on the basis of the oxygen deficiency with enhanced of Sr^{2+} ion ratio. However, the values obtained were nearly similar to the given values of LSMO films grown on the various substrates in which the values were in the range of 2.06 to 2.46.[35] Otherwise, both static and high frequency dielectric constants are determined for all the samples. The high frequency dielectric constant ($\mathbf{\varepsilon}_\alpha$) is calculated using the relation[33]:

$$\mathbf{\varepsilon_\alpha = n^2} \qquad \textit{(Equation 3)}$$

Where 'n' is the refractive index.

The static dielectric constant ($\mathbf{\varepsilon}_0$) of the samples is calculated using the relation:[33]

$$\mathbf{\varepsilon_0 = 18.52 - 3.08\, E_g} \qquad \textit{(Equation 4)}$$

Where Eg is the band gap energy. The calculated values of $\mathbf{E_g}$, **n**, $\mathbf{\varepsilon_\alpha}$ and $\mathbf{\varepsilon_0}$ for different samples are presented in Table 1. Apparently, the values of $\mathbf{\varepsilon}_\alpha$ and ε_0 were decreased with increasing the Sr^{2+} ion content. The results can be discussed on basis of polaron hopping mechanism, charge transported by the Mn^{3+}–O–Mn^{4+} network. The partial replacement of La^{3+} by Sr^{2+} in LSM created polarons due to the conversion of Mn^{3+} to Mn^{4+} so as to achieve the electroneutrality. The concentration of polaron was increased with an increase in Sr content in LSM thereby the dielectric constant was decreased[36].

Table 1. Values of E_g, **n**, $\mathfrak{E}_\alpha$ and $\mathfrak{E}_0$ of lanthanum strontium manganite nanopowders prepared by the co-precipitation method at different Sr^{2+} ion molar ratios

Sample ID	E_g	n	$\mathfrak{E}_\alpha$	$\mathfrak{E}_0$	Crystallite size (nm)
LSM2	2.42	2.50	6.25	11.06	25
LSM5	2.62	2.45	6.00	10.45	38
LSM8	2.80	2.41	5.80	9.89	42

6. Magnetic properties

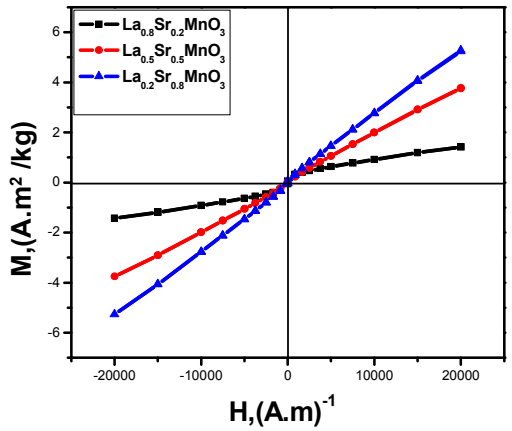

Fig. 7 The Ferromagnetic hysteresis curves for LSM nanopowders synthesized using co-precipitation method with different Sr^{2+}ion contents and annealed at 1000°C for 2 h.

The magnetic properties of the lanthanum strontium manganite $La_{1-x}Sr_xMnO_3$ synthesized through co-precipitation method with different strontium ion contents (x= 0.2, 0.5 and 0.8) are presented in Figure 7. From the hysteresis loops, the magnetic parameters such as saturation magnetization (*Ms*), remanent magnetization (*Mr*) and coercive field (*Hc*) are recorded in Table 2. Evidently, S-shaped loop was observed for low Sr^{2+} ion concentration which has the low saturation magnetization (*M*s = 1.42 $A.m^2/kg$) and the high coercivity (Hc=150.02 Am^{-1}). Otherwise, further increasing of the Sr^{2+} ion content to 0.5 was found to increase the saturation magnetization (Ms= 3.76 $A.m^2/kg$) and decrease the corecivity to 69.31 $A.m^{-1}$. Meanwhile at high Sr^{2+} ion molar ratio, high saturation magnetization (5.2 $A.m^2/kg$) was accomplished whereas middle coercivity 104.2 $A.m^{-1}$ was fulfilled. Plainly, the weak ferromagnetic as well as multiphase (ferromagnetic and paramagnetic) nature was observed for all tested samples. The results were agreement with the previous published result by Zhou *et al.*[37]

However, the saturation magnetization was particle size dependent. It was found that the saturation magnetization was increased with increasing the particle size as the further increasing of Sr^{2+} ion content. For instance, the surface magnetic anisotropy originating from a magnetically disordered surface layer known as a dead or passivating layer existed in the nanoparticles is usually the evidence of the phenomenon. With decreasing particle sizes, the thickness of the passivating layer and the number of disordered spins increases, which are adverse to the ferromagnetic order, thus leading to the reduction of magnetization and the increase of *Hc* and *Mr*. However, the reduction of magnetic coercivity significantly depends on their magneto-crystalline anisotropy, micro-strain, inter-particle interaction, size and shape[38-40].

The magnetic moment per molecule (nB) was obtained as summarized in Table 2 using the empirical formula[40]

$$nB = \frac{Mw \times Ms}{5585} \qquad (Equation\ 5)$$

Where M_W is the molecular weight, M_s is the saturation magnetization and 5585 is the magnetic factor. It was demonstrated that the calculated nB values were increasing with increment of Sr^{2+} ion molar ratio.

Table 2. Room temperature saturation magnetization (*M*S), remnent magnetization, coercivity (*Hc*) and Bohr magneton for LSM nanopowders prepared by co-precipitation method

Sample ID	*Ms* ($A.m^2$ /kg)	*Mr* ($A.m^2$ /kg)	*Hci* (Am^{-1})	Bohr magneton ($A.m^2$ /kg)
$La_{0.8}Sr_{0.2}MnO_3$	1.4252	0.0629	150.02	0.059
$La_{0.5}Sr_{0.5}MnO_3$	3.7619	0.0216	69.318	0.145
$La_{0.2}Sr_{0.8}MnO_3$	5.2772	0.0429	104.20	0.189

7. Electrochemical impedance spectroscopy measurements

Electrochemical impedance spectroscopy (EIS) was also performed under open circuit voltage (OCV) conditions, in order to analyze the different limiting steps contributing to the cell polarization. An inductive loop is usually observed at low frequencies and can be attributed to the activation of a passive layer at the electrode surface[41]. The analysis of the Nyquist diagrams is extremely complex[42]. Impedance spectra of LSM electrodes correspond to at least two overlapping depressed arcs, one associated with bulk or surface diffusion and the other associated with surface exchange of oxygen and charge transfer.[43, 44]

Figure 8 shows the Nyquist AC impedance plots of the LSM cell measured with different molar ratios of strontium. The highest frequency intercept on the real axis of Nyquist EIS spectra represented the total specific ohmic resistance (RΩ), and the distance between the lowest and the highest frequency intercepts corresponded to the total area specific polarization resistance (Rp) from both anode and cathode. The LSM cell showed drastically increased Rp values from 3.10 to 5.21, and 8.56 Ω cm^2 at 0.2, 0.5, and 0.8 molar ratios of strontium ions. This suggests that the total area specific polarization resistance (Rp) from both anode and cathode was largely increased by increasing the molar ratio of strontium ions. Furthermore, this suggests a better interfacial contact between the electrolyte and cathode. The impedance spectra plotted in figure 7 were analyzed by fitting the data with the equivalent circuit shown in Scheme 1. In this scheme, L corresponds to an inductance, which is usually associated with the platinum current/voltage probes, or to the high-frequency phase shift of the electrochemical equipment; Re is the ohmic resistance of the electrolyte which interpreted as the sum of grain and grain boundary resistance; (R1, CPE1) and (R2, CPE2) correspond to the high- and low-frequency arcs, respectively. The circuit may be described by the following equation: $R_e(R_1Q_1)(R_2Q_2)$ where R is a resistance and Q the constant phase element (CPE)[41].

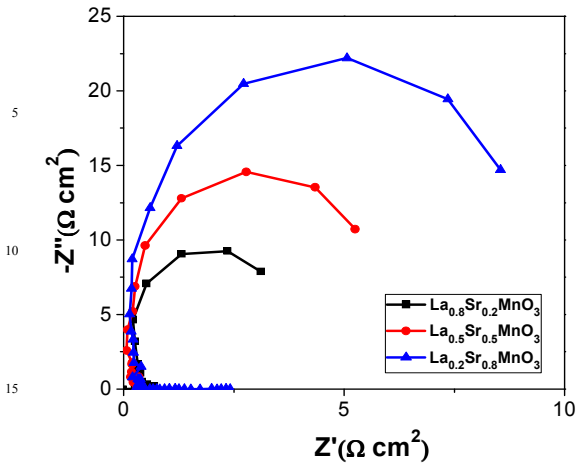

Fig. 8 Nyquist plots (Z' vs. Z″) of LSM prepared by the co-precipitation method and annealed at 1000°C for 2h with different Sr^{2+} ion molar ratios (0.2, 0.5 and 08).

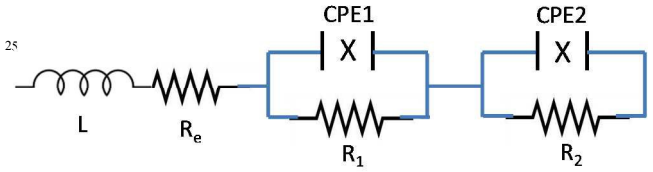

Scheme 1. Schematic representation of the equivalent circuit employed to fit the impedance data

Conclusions

$La_xSr_{1-x}MnO_3$ nanopowders with *x*= 0.2, 0.5 and 0.8 have been synthesized using co-precipitation method based on methyl amine as base for the first time. This technique gives more homogeneous and uniform structure than that obtained by the other methods as well as this method is simple, low cost and time saving. Obviously, the XRD profiles revealed that the pure monoclinic $La_xSr_{1-x}MnO_3$ phase could be obtained from the precipitated precursors at pH 12 by annealing at 1000°C for 2h. The Sr^{2+} ion content has significant effect on the surface morphology. SEM images indicated that tablet like structure was observed at low Sr^{2+} ion content. Clearly, the obtained powder was highly agglomerated and exhibits grains in nanometeric size range. Meanwhile, the band gap energy was increased from 2.42 to 2.80 eV when increasing the Sr^{2+} ion content from 0.2 to 0.8. Of note, the refractive index n was slightly decreased from 2.50 to 2.41 with increasing the Sr^{2+} ion molar ratios. Prominently, the high frequency dielectric constant (ε_α) and the static dielectric constant (ε_0) were decreased with increasing the Sr^{2+} ion molar ratios. On other hand, the saturation magnetization (*Ms*) and the Bohr magneton were enhanced with further increasing the Sr^{2+} ion concentration. Overall, these materials could have applications in different fields such as cathode materials in solid oxide fuel cell.

Notes and references

[a]*Central Metallurgical Research & Development Institute, P.O. Box: 87 Helwan, Cairo, Egypt*
[b]*Faculty of Science, Chemistry department, Al-Azhar University, Nasar City , Egypt*
[c]*Institut Européen des Membranes, UMR5635 CNRS-UM-ENSCM, Place Eugène Bataillon, 34095 Montpellier cedex 5, France*
Corresponding author: ali_omar155@yahoo.com

1. M. Balaguer, V. B. Vert, L. Navarrete and J. M. Serra, *Journal of Power Sources*, 2013, **223**, 214-220.
2. F. Bidrawn, G. Kim, N. Aramrueang, J. M. Vohs and R. J. Gorte, *Journal of Power Sources*, 2010, **195**, 720-728.
3. K. Chen, Z. Lü, X. Chen, N. Ai, X. Huang, X. Du and W. Su, *Journal of Power Sources*, 2007, **172**, 742-748.
4. S. Giraud and J. Canel, *Journal of the European Ceramic Society*, 2008, **28**, 77-83.
5. H. A. Hamedani, K.-H. Dahmen, D. Li, H. Peydaye-Saheli, H. Garmestani and M. Khaleel, *Materials Science and Engineering: B*, 2008, **153**, 1-9.
6. A. A. Rabelo, M. C. de Macedo, D. M. de Araujo Melo, C. A. Paskocimas, A. E. Martinelli and R. M. do Nascimento, *Materials Research-Ibero-American Journal of Materials*, 2011, **14**, 91-96.
7. W. J. d. Silva, D. M. d. A. Melo, S. F. d. C. X. Soares, P. M. Pimentel, R. M. d. Nascimento, A. E. Martinelli and A. A. Rabelo, *Matéria (Rio de Janeiro)*, 2007, **12**, 65-71.
8. R. Doshi, V. L. Richards, J. D. Carter, X. P. Wang and M. Krumpelt, *Journal of the Electrochemical Society*, 1999, **146**, 1273-1278.
9. S. M. Haile, *Acta Materialia*, 2003, **51**, 5981-6000.
10. S. Maity, S. K. Ray and D. Bhattacharya, *Journal of Physics and Chemistry of Solids*, 2013, **74**, 315-321.
11. M. Mori, N. M. Sammes, E. Suda and Y. Takeda, *Solid State Ionics*, 2003, **164**, 1-15.
12. J. Sfeir, S. Vaucher, P. Holtappels, U. Vogt, H. J. Schindler, J. Van herle, E. Suvorova, P. Buffat, D. Perret, N. Xanthopoulos and O. Bucheli, *Journal of the European Ceramic Society*, 2005, **25**, 1991-1995.
13. L. Conceicao, C. R. B. Silva, N. F. P. Ribeiro and M. Souza, in *Solid Oxide Fuel Cells 11*, eds. S. C. Singhal and H. Yokokawa, Electrochemical Soc Inc, Pennington, 2009, vol. 25, pp. 2301-2308.
14. M. Marinsek, K. Zupan, T. Razpotnik and J. Macek, *Materiali in Tehnologije*, 2007, **41**, 85-90.
15. C. R. Xia, Y. L. Zhang and M. L. Liu, *Electrochemical and Solid State Letters*, 2003, **6**, A290-A292.
16. A. O. Stoermer, J. L. M. Rupp and L. J. Gauckler, *Solid State Ionics*, 2006, **177**, 2075-2079.
17. M. B. Kakade, S. Ramanathan and P. K. De, *British Ceramic Transactions*, 2003, **102**, 211-215.
18. M. R. Cesario, D. A. Macedo, R. M. P. B. Oliveira, P. M. Pimentel, R. L. Moreira and D. M. A. Melo, *Journal of Ceramic* Processing Research, 2011, 12, 102-105.
19. A. O. Turky , M.M. Rashad , M. Bechelany , Materials and Design 1016,90, 54–59.
20. M M Rashad, D. A. Rayan, A.O. Turky, M. M. Hessien, J. Magn. Magn. Mater. 2015,374,359-366
21. M. Zhi, G. Zhou, Z. Hong, J. Wang, R. Gemmen, K. Gerdes, A. Manivannan, D. Ma and N. Wu, Energy & Environmental Science, 2011, 4, 139-144.
22. M. M. Rashad, S.M. El-Sheikh, Mater. Res. Bull. 2011, 46,469-477
23. P. Kulandaivelu, K. Sakthipandi, P. Senthil Kumar and V. Rajendran, Journal of Physics and Chemistry of Solids, 2013, 74, 205-214.
24. I. Bergenti, V. Dediu, M. Murgia, A. Riminucci, G. Ruani and C. Taliani, Journal of Luminescence, 2004, 110, 384-388.
25. C. N. R. Rao, A. Arulraj, P. N. Santosh and A. K. Cheetham, Chemistry of Materials, 1998, 10, 2714-2722.
26. R. Vonhelmolt, J. Wecker, B. Holzapfel, L. Schultz and K. Samwer, Physical Review Letters, 1993, 71, 2331-2333.
27. M. Cesaria, A. P. Caricato, G. Leggieri, M. Martino and G. Maruccio, Thin Solid Films, 2013, 545, 592-600.
28. M. M. Rashad, A. O. Turky and A. T. Kandil, Journal of Materials Science-Materials in Electronics, 2013, 24, 3284-3291.

29. A. O. Turky, M. M. Rashad, Z. I. Zaki, I. A. Ibrahim and M. Bechelany, RSC Advances, 2015, 5, 18767-18772.
30. M. P. de Jong, V. A. Dediu, C. Taliani and W. R. Salaneck, Journal of Applied Physics, 2003, 94, 7292-7296.
31. K. Takenaka, Y. Sawaki, R. Shiozaki and S. Sugai, Physical Review B, 2000, 62, 13864-13867.
32. R. G.Tanguturi, T. Bora, S. Ravi, D. Pamu, Physics Procedia 2014, 54,70-74
33. T. S. Moss, physica status solidi (b), 1985, 131, 415-427.
34. P. Herve and L. K. J. Vandamme, Infrared Physics & Technology, 1994, 35, 609-615.
35. A. A. Tikhiib , S. V. KaraMurzaa , Yu. M. Nikolaenkob , V. A. Gritskikha , N. V. Korchikovaa , I. V. Zhikharevb, Inorganic Materials, 2015, 51, 928–932.
36. K. R. Nagde , S. S. Bhoga Ionics 2009, 15, 571–578
37. Y. Zhou, X. Zhu, S. Li, Phys. Chem. Chem. Phys., 2015, 17, 31161
38. A. O. Turky, M. Mohamed Rashad, A. E.-H. Taha Kandil and M. Bechelany, Physical Chemistry Chemical Physics, 2015, 17, 12553-12560.
39. K. P. Shinde, S. S. Pawar, P. M. Shirage and S. H. Pawar, Applied Surface Science, 2012, 258, 7417-7420.
40. M. M. Rashad, M. G. Fayed, T. M. Sami and E. E. El-Shereafy, Journal of Materials Science-Materials in Electronics, 2015, 26, 1259-1267.
41. J. Im, I. Park and D. Shin, Ceramics International, 2014, 40, 5567-5573
42. A. Esquirol, N. P.Brandon, J. A.Kilner, M. J. Mogensen, Electrochem. Soc. 2004, 151, A1847
43. M. A. L.-Bercero, J. A. Kilner , S. J. Skinner, Chem. Mater, 2010, 22,1134-1141
44. K. Chen, N. Ai, S. P. Jiang, Int. J. of Hydrogen Energy 2012,37,1301-1310

Graphical abstract

We report on the synthesis and characterization of lanthanum strontium manganite with tunable optical, magnetic and electrical properties